2013

Roughness analysis applied to niobium thin films grown on MgO(001) surfaces for superconducting radio frequency cavity applications

D. B. Beringer
William & Mary

R. A. Lukaszew
William & Mary, ralukaszew@wm.edu

W. M. Roach
William & Mary

C. Clavero
William & Mary

C. E. Reece

Recommended Citation

Beringer, D. B., Roach, W. M., Clavero, C., Reece, C. E., & Lukaszew, R. A. (2013). Roughness analysis applied to niobium thin films grown on MgO (001) surfaces for superconducting radio frequency cavity applications. Physical Review Special Topics-Accelerators and Beams, 16(2), 022001.

Roughness analysis applied to niobium thin films grown on MgO(001) surfaces for superconducting radio frequency cavity applications

D. B. Beringer,[1] W. M. Roach,[2] C. Clavero,[2] C. E. Reece,[3] and R. A. Lukaszew[1,2]

[1]*Department of Physics, The College of William & Mary, Williamsburg, Virginia 23187, USA*
[2]*Department of Applied Science, The College of William & Mary, Williamsburg, Virginia 23187, USA*
[3]*Thomas Jefferson National Accelerator Facility, Newport News, Virginia 23606, USA*

(Received 30 November 2011; published 5 February 2013)

This paper describes surface studies to address roughness issues inherent to thin film coatings deposited onto superconducting radio frequency (SRF) cavities. This is particularly relevant for multilayered thin film coatings that are being considered as a possible scheme to overcome technical issues and to surpass the fundamental limit of ~50 MV/m accelerating gradient achievable with bulk niobium. In 2006, a model by Gurevich [Appl. Phys. Lett. **88**, 012511 (2006)] was proposed to overcome this limit that involves coating superconducting layers separated by insulating ones onto the inner walls of the cavities. Thus, we have undertaken a systematic effort to understand the dynamic evolution of the Nb surface under specific deposition thin film conditions onto an insulating surface in order to explore the feasibility of the proposed model. We examine and compare the morphology from two distinct Nb/MgO series, each with its own epitaxial registry, at very low growth rates and closely examine the dynamical scaling of the surface features during growth. Further, we apply analysis techniques such as power spectral density to the specific problem of thin film growth and roughness evolution to qualify the set of deposition conditions that lead to successful SRF coatings.

DOI: 10.1103/PhysRevSTAB.16.022001 PACS numbers: 74.78.−w, 74.62.Bf, 68.55.−a

I. INTRODUCTION

Most radio frequency (rf) cavities used in particle accelerators are made from conventional conductors, such as copper, whereas a few large research accelerators like the Continuous Electron Beam Accelerator Facility (CEBAF) at Thomas Jefferson National Accelerator Facility (TJNAF), the Spallation Neutron Source (SNS), and the European X-FEL currently under construction utilize superconducting radio frequency (SRF) accelerating cavities made of bulk Nb. The performance of such SRF cavities is almost entirely determined by a thin layer on the inner surface approximately 40 nanometers thick. While the technology has matured to the point of reliably producing the quality factors of $>10^{10}$ and accelerating gradients larger than 35 MV/m, the inner workings of most of the implemented processes applied on bulk Nb cavities (such as buffered chemical polishing, electropolishing, low T baking, hydrofluoric acid rinsing) to achieve the best performance traits remain unclear. Thus, the ultimate role of surface roughness and lossy impurities has eluded fundamental understanding. Yet, due to the fact that SRF technology is a surface phenomenon because of the very shallow penetration depth of the rf fields, there is also interest in developing thin film coatings for SRF cavities to reduce costs and to improve thermal efficiency.

A. SRF cavities and superconducting thin films

The earliest work on Cu cavities coated with Nb thin films was done at CERN [1]. Further, tests in the thin film cavities used at the LEP-II collider after this pioneer work indicated that there was significant drop in Q above a 15 MV/m accelerating gradient at 1.5 GHz and 1.7 K [2]. Since these attempts using superconducting thin film coatings have shown poor SRF performance, mainly ascribed to the microstructure of the films, the challenge has remained to understand the dependence of the SRF properties on the detailed characteristics of ''real'' surfaces and then to employ appropriate techniques to tailor the surface properties for greatest benefit. Several material factors contribute to the degradation of the SRF performance with respect to ''ideal'' surfaces, and among others, surface topography contributes local field enhancements, which effectively lowers the sustainable critical field and allows early fluxoid entry and thus increased dissipation. In a recent publication, Krishnan *et al.* presented advances for the deposition of Nb films onto SRF cavities using energetic condensation [3]. Their results pointed to an alternative way to coat cavities where a high flux of Nb ions combined with the high-energy deposition into the first few monolayers of the substrate was shown capable of inducing significant modification of that surface. In their work they noted that good quality Nb films were those that were epitaxially grown onto MgO crystalline substrates.

The quest for thin film SRF surfaces with improved performance does not stop with Nb thin film coatings since several laboratories, including ours, are working on the development of multilayered thin film superconductor technology that could overcome the fundamental limit of $\sim$50 MV/m accelerating gradient attainable with bulk niobium. In fact, field gradients >100 MV/m are of great interest, but no simple material is known to be capable of sustaining such performance [4]. In this multilayer model, superconducting layers with thickness less than the penetration depth are intercalated with insulating barriers and stacked over the Nb surface [5]. A simplistic scenario where, for example, a single Nb_3Sn layer of thickness $d =$ 50 nm is deposited over Nb with a dielectric layer in between, can provide enough shielding so that the breakdown field is doubled with respect to bulk Nb. Thus, the possibility of using multilayered thin film coatings to push accelerating field gradients and, in particular, superconducting/insulating/superconducting (SIS) multilayer structures incorporating other superconductors with higher critical field and with suitable shielding thickness, represents a promising material solution which may overcome intrinsic SRF limitations arising from using bulk superconductors.

Since the thickness involved in these structures must be less than the rf penetration length in order to provide adequate shielding, slower growth methods that allow for controlled epitaxial thin film growth—magnetron sputtering methods, for instance—may be ideal for the practical and experimental realization of this SIS multilayer model. Yet, systematic research is needed to understand the actual correlation between the surface characteristics and the consequent SRF performance for any thin film coating approach to work. Thin film nucleation and subsequent growth kinetics influence epitaxial thin film growth on different surfaces making the superconducting properties of film coatings differ from those in bulk. This is primarily because of the limited material supply inherent to a thin film geometry, as well as stress contributions due to lattice mismatch between film and substrate, which can induce significant surface roughness. Understanding the evolution of rough surfaces during deposition of thin films is therefore paramount since it has already been shown that rough surfaces lead to undesirable effects for SRF performance that can be minimized with suitable choices of growth parameters.

Here we investigate experimentally the evolution of the surface morphology of Nb films grown on a typical insulating surface such as MgO and apply models of roughness evolution to investigate the surfaces in question and apply power spectral density (PSD) analysis, which has also been used in the SRF context to study bulk Nb surfaces after various processes and chemical treatments [6]. In our present studies we used DC magnetron sputtering techniques to prepare films, but it is worth noting that the possibility of tuning the deposited Nb microstructure and morphology with higher adatom/ion energy is an attractive approach towards further controlling the interfaces of viable thin film coatings [7]. Thus, we point out that the analytical methodology mentioned in this report will be equally applicable to films obtained with such techniques and would offer a suitable comparison platform.

B. Nucleation and growth

The structure zone diagram (SZD) presented by Thornton [8] that describes the interplay between thermal

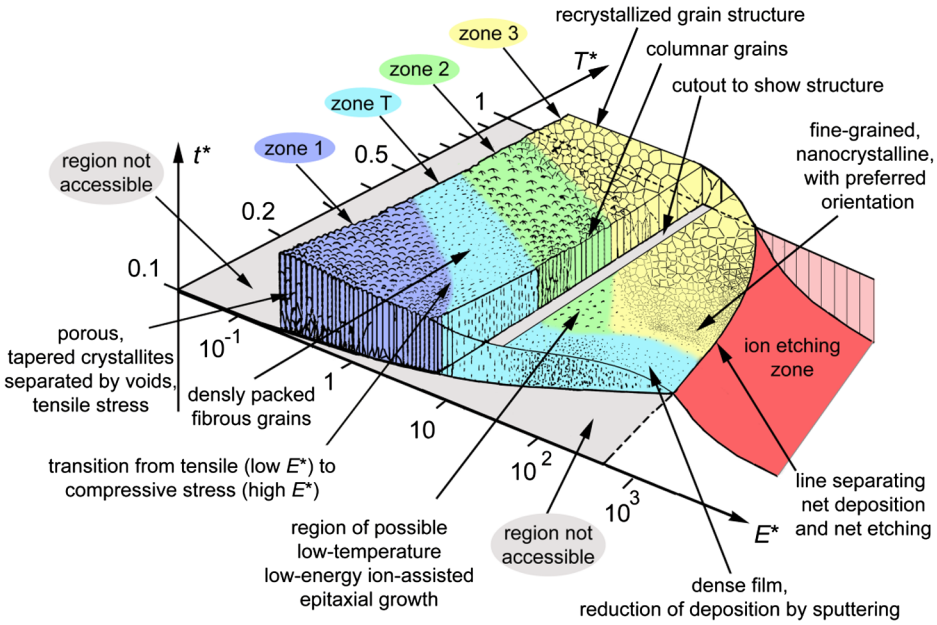

FIG. 1. Modified SZD diagram (reproduced from Ref. [9] with permission from the author and Elsevier Publishers). We notice a window of parameters where it is possible to achieve epitaxial growth.

and kinetic energy driven film growth in sputtered thin films, has been recently extended by Anders to include other possibilities related to additional thin film deposition techniques (Fig. 1) [9]. This diagram considers a region where nonpenetrating ions (or atoms) may have enough energy to promote surface diffusion. Thus, there is an interesting energy window where the particle's kinetic energy is between the surface displacement energy and bulk displacement energy: epitaxial growth is promoted because no defects are created in the film bulk. Since epitaxial modes of growth are commonly divided into three parts [Frank-Van Der Merve: layer growth two-dimensional (2D); Stranski-Krastanov: complete monolayer plus 3D clusters; Wolmer-Weber: island growth (3D)], the nucleation phenomena of thin films have to be taken into account. It is well known that the parameters affecting the growth and that can strongly influence the morphological and structural behaviors of the layer are the growth rate, the substrate temperature, sputtering pressure, film thickness, and ion-to-atom ratio. Adequate control is surely valuable for the nucleation of the first sublayer on the substrate and it is of paramount importance when attempting a multilayered coating (see Fig. 2) since the growth mechanism peculiar to each sputtered material can be strongly modified since roughness and topography never stop changing after the deposition of each sublayer [10].

The physical processes that can significantly affect early nucleation are the presence and degree of step-edge diffusion barriers and strain relaxation mechanisms due to mismatch between film and substrate lattice parameters [11,12]. In addition, the evolution of the surface during epitaxial growth can lead to faceting, further hindering the possibility of smooth surfaces. Thus, the growth mode during the nucleation stage can affect the ultimate surface morphology with fractal characteristics whose self-similarity, i.e., self-affinity, persists throughout the temporal and spatial surface evolution during subsequent growth and has a profound effect on relevant physical properties. In the following sections, we first describe our experimental configuration, characterization methods, and we discuss the various analytical formalisms that have been proposed to model surface roughness evolution in order to have a suitable tool to qualify a given set of thin film experimental deposition conditions.

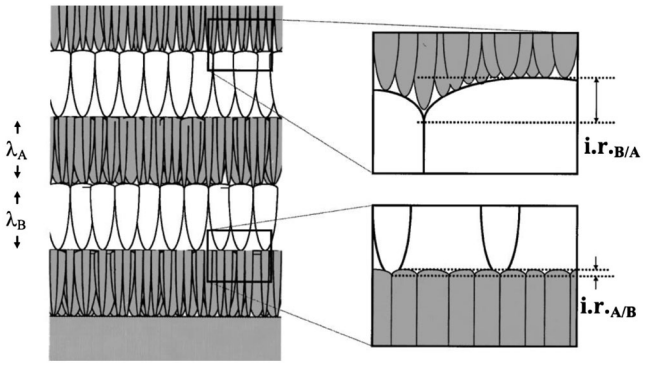

FIG. 2. Cross-sectional illustration of a hypothetical multilayer coating formed with equal λA and λB thicknesses. A difference of nucleation density between materials A and B can be noticed. This one induces a surface smoothening or a reverse effect according to the deposited sublayer and so, interfacial roughness (i.r. in the figure) can be strongly modified (reproduced from Ref. [10] with permission from the American Institute of Physics).

II. EXPERIMENTAL

In order to tackle the analysis of the nucleation and growth of thin films onto specific surfaces, the thin film deposition geometry must be very well defined since it can determine the degree of reproducibility between experimental runs, such that comparisons between samples are meaningful. The deposition system used for this study is a modified ultrahigh vacuum (UHV) Perkin-Elmer molecular beam epitaxy system, shown in Fig. 3, with five source ports outfitted with sputtering guns. The system is equipped with a cryopump to enable adequate pumping speed for the sputtering process in the mTorr range.

Our test samples were epitaxial Nb films grown on MgO(001) substrates in an ultrahigh vacuum (UHV) deposition system with a base pressure in the high 10^{-10} Torr range. The films were prepared via DC magnetron sputtering of a 2-inch Nb target of 99.95% purity. Prior to deposition, each polished MgO substrate was *in situ* annealed for 1 h at 600°C to degas and recrystallize the surface. The subsequent growth of each film was carried out at a growth temperature of 600°C. Two Nb film thickness series, with film thickness ranging from 10 to 1000 nm, were prepared under similar deposition conditions. Series 1 films (demonstrating a two-phase crystallographic structure) were deposited using DC magnetron sputtering with an argon working gas pressure of 1.0 mTorr. Series 2 films (demonstrating a single crystal structure) were sputtered at 5.0 mTorr. The DC power delivered to the Nb target was 60 W. Growth rates for the thin films, as determined by x-ray reflectivity and ellipsometry, were 0.32 Å/sec for Series 1 and 0.48 Å/sec for Series 2.

In order to investigate the role of the initial substrate surface on the nucleation process, we investigated Nb films deposited on MgO substrates that were only *in situ* annealed (Series 1) and substrates where a thin and fresh seed layer (~ 2 nm) of MgO was grown onto the substrate using reactive sputtering. A higher working gas pressure or an increased sputtering power—are tunable parameters that also influence the growth of the single crystal films—both lead to a corresponding increase in the growth rate (note: we used increased pressure in Series 2). All the films were investigated with *in situ* reflection high-energy electron diffraction (RHEED), and *ex situ* atomic force microscopy (AFM) described in the following section.

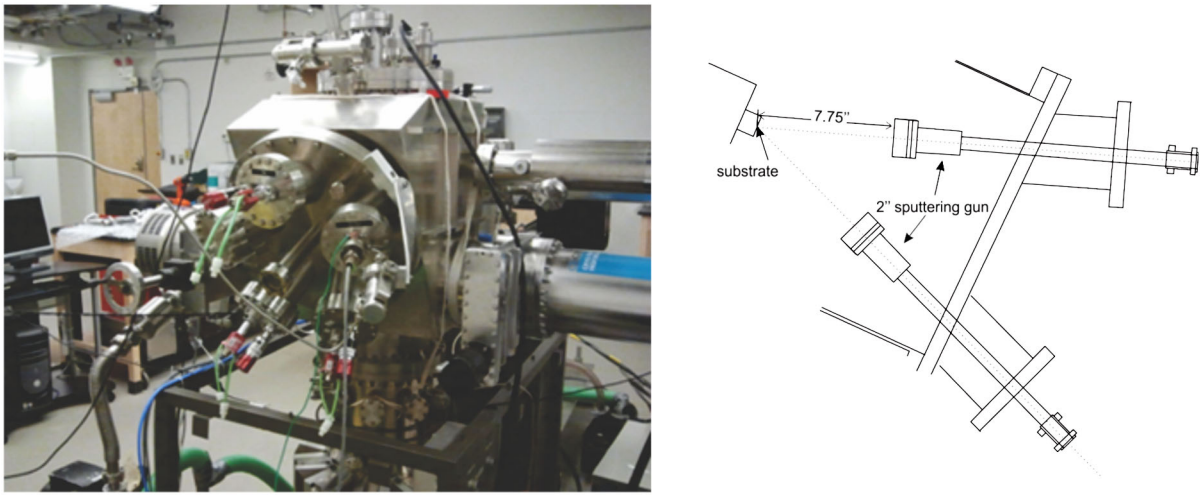

FIG. 3. Left: Rear view of the Perkin-Elmer deposition chamber where we note five source ports with confocal geometry. Right: Diagram showing the relative position of two of the five sputtering sources with respect to the substrate.

A. Surface characterization tools

RHEED is a surface sensitive diffraction technique where an electron beam at glancing angle incident geometry can provide *in situ* qualitative and quantitative information about the surface microstructure and morphology after diffracting from the surface onto a phosphor screen [13]. We note that since Nb growth over MgO substrates proceeds in 3D fashion, i.e., Volmer-Weber mode; RHEED cannot be used as an effective means to extract growth rates and thickness via recording intensity oscillations of the electron beam [14]. Thus, RHEED was employed mainly to obtain *in situ* information regarding the evolution of the film microstructure, including the epitaxial registry of the Nb films on MgO, as well as the strain evolution and surface faceting of Nb films deposited on MgO substrates as well as sapphire which are described elsewhere [15]. Characteristic RHEED patterns were collected for each film along two distinct crystallographic directions corresponding to MgO[100] and MgO[110] azimuths.

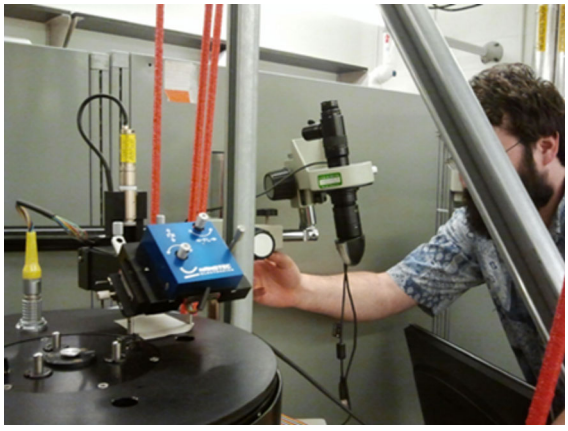

FIG. 4. *Ex situ* AFM. The system is mechanically isolated from the ground by stiff springs in order to minimize vibration-induced noise in the topographic images.

Ex situ AFM was the main tool used for the characterization of the surface morphology as well as its evolution with film thickness for the present study (Fig. 4). AFM images were collected with a Nanotec Cervantes AFM immediately upon removal from the UHV system in order to capture representative surface images for each sample prior to significant oxidation upon exposure to atmospheric conditions. The AFM was operated in noncontact with an AppNano ACTA AFM tip that has a nominal tip diameter of less than 10 nm. The free software WSxM from Nanotec was used for the analysis of the AFM images [16]. Line scans, self-correlation functions, Fourier transforms, root mean square (rms) roughness and PSD functions native to the Nanotec WSxM software were used in the processing and analysis of the AFM images. Line scans in conjunction with 2D self-correlation were utilized to extract global and local anisotropic lateral correlation lengths (i.e. average island size and separation) as well as rms information over short length scales, rms roughness data, representing the surface interface width, were obtained from the AFM topography images. The WSxM PSD package was used to determine the average spectral features of the thin films.

III. SCALING ANALYSIS: DYNAMIC EVOLUTION OF SURFACES

As we have emphasized previously, the success of epitaxial SIS multilayer structures, from a practical point view, depends on our ability to understand and control the morphology and structure at each interface. Generally speaking, as a surface evolves in time and space via stochastic processes (such as chemical etching or ballistic deposition), the surface will coarsen. The task of understanding and quantifying this dynamic evolution of growth fronts is translated into questions regarding the relative

spatial and temporal scaling relationships between similar, persistent, characteristic features, and their associated length scales throughout the development of the surface—specifically, the correlation between certain characteristic lengths both parallel and perpendicular to the direction of the evolving growth front. The scaling behavior can be quantified in the form of scaling exponents that collectively encapsulate the energetic and kinematic mechanisms responsible for the coarsening surface. In what follows we briefly discuss the most relevant aspects of dynamical scaling for the evaluation of SIS/SRF surfaces.

In the simplest models, the dynamical scaling of a surface can be described by a finite set of global scaling parameters; quantitatively, the dynamic evolution of the roughness of the system in question can be fully described by a pair of scaling exponents, α and β, the global roughness exponent and growth exponent, respectively. For a comprehensive review and formal discussion of the theory, we direct the reader to the seminal work by Family-Vicsek [17]. It is assumed that stochastic processes drive the surface evolution and that the resulting features will possess a self-affine form; however, real surfaces may exhibit so-called "anomalous" scaling behavior (i.e. possess disparate global and local scaling qualities when the surface is examined over different length scales) that cannot be fully described by this limited set of parameters. General dynamical scaling applies a more generic set of scaling assumptions, formulated in Fourier space, which introduces an additional and independent scaling parameter that can be used to classify anomalous scaling into invariant subclasses [18]. Here the scaling assumption is that the power spectral density (PSD) defines a structure factor S

$$S(\boldsymbol{k}, t) = \langle H(\boldsymbol{k}, t) H(-\boldsymbol{k}, t) \rangle, \tag{1}$$

where H is the Fourier transform of the surface height function, k is the spatial frequency, and t represents a temporal parameter (in the case of constant growth rate, film thickness is an adequate choice of parameter). $S(k, t)$ assumes the general form (for a 2 + 1 dimensional system)

$$S(k, t) = k^{-(2\alpha_s + 2)} t^{2(\alpha_{\mathrm{loc}} - \alpha_s)/z} \tag{2}$$

and the spectral exponent α_s quantitatively captures the anomalous scaling independent of local and global values for α and β. The value of the spectral exponent, evaluated from the slope of the log-log plot S vs k in the realm of large k, demarcates scaling behavior by

$$\begin{aligned} \alpha_s < 1 \Rightarrow \alpha_{\mathrm{loc}} = \alpha_s \begin{cases} \alpha_s = \alpha \Rightarrow \text{Family-Vicsek} \\ \alpha_s \neq \alpha \Rightarrow \text{intrinsic} \end{cases} \\ \alpha_s > 1 \Rightarrow \alpha_{\mathrm{loc}} = 1 \begin{cases} \alpha_s = \alpha \Rightarrow \text{super-rough} \\ \alpha_s \neq \alpha \Rightarrow \text{new class.} \end{cases} \end{aligned} \tag{3}$$

Hence, general dynamic scaling can be used to classify the evolution of a surface, under a particular set of growth parameters, into a scaling universality class.

In the context of evaluating the surface morphology for candidate thin film surfaces for SIS/SRF applications, we emphasize that general dynamic scaling provides a means to quantify, identify, and compare roughness trends and final morphological traits of particular thin film growth processes. For instance, it is advantageous to understand whether certain growth conditions lead to extremely rough surfaces, like those exemplified by the aptly named "super-rough" universality class, which will be detrimental to the development of viable multilayer epitaxial structures where subsequent growth is critically sensitive to surface morphology.

IV. EXPERIMENTAL RESULTS

RHEED images taken along two distinct azimuthal directions in the Nb/MgO system indicate an epitaxial, mixed-phase Nb structure where Nb(110)/MgO(001) is

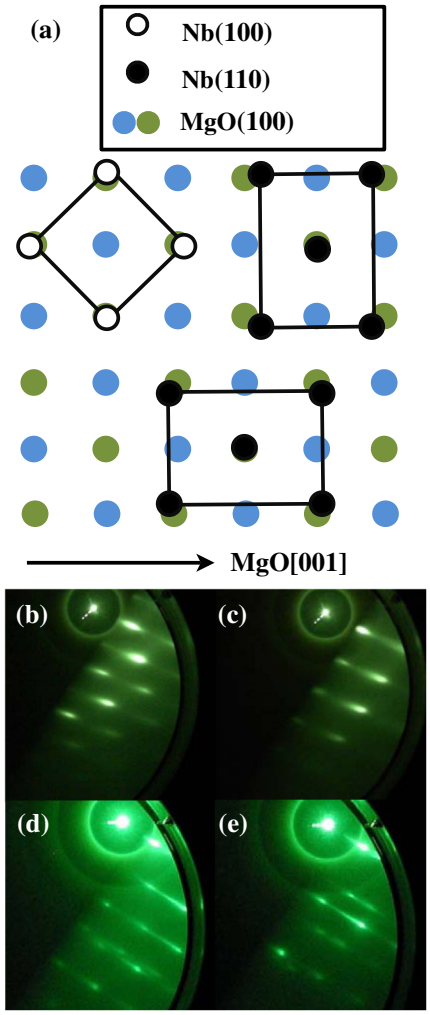

FIG. 5. (a) Atomic representation of epitaxial registry of Nb films with respect to the MgO(001) substrate. (b) RHEED image of 100 nm single crystal Nb(100)/MgO(001) taken along the MgO[011] azimuth and (c) along the MgO[001] azimuth. (d) RHEED image of the 100 nm Nb Film taken along the MgO[011] azimuth and (e) along the MgO[001] azimuth.

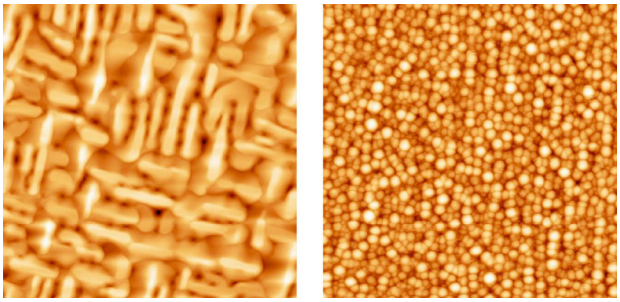

FIG. 6. Left: Representative 2 μm $\times$ 2 μm AFM scan from Series 1 for 600 nm Nb films. Right: Representative 2 μm $\times$ 2 μm AFM scan from Series 2 for a 1000 nm film.

present with two possible in-plane azimuthal crystalline orientations for Series 1. In contrast, the RHEED images from Series 2 show a single crystal Nb structure with Nb(100)/MgO(001) where Nb[100]||MgO[100] (Fig. 5). The observation that Nb achieves these particular registries with the underlying MgO(001) substrate is consistent with literature [19]. The determination of which particular epitaxial Nb registry is achieved between Series 1 and Series 2 films is highly sensitive to the initial substrate conditions as well as the growth rate and sputtering pressure.

The surface morphology of the films was investigated using AFM. The horizontal direction in each AFM scan was taken as close as possible to parallel to the MgO[001] direction. In Series 1, a clear biaxial morphological anisotropy is manifest (Fig. 6, left) and suggestively, the direction and relative orientation of the morphological anisotropic features are consistent with structural anisotropies observed in the corresponding RHEED patterns. In stark comparison, the AFM scans from Series 2 show a more isotropic surface morphology (Fig. 6, right) devoid of the interwoven, anisotropic island features observed in Series 1 films. A comparison of the rms roughness for the thickest films—6.7 nm for the 600 nm film from Series 1 and 5.9 nm for the 1000 nm film from Series 2—in addition to the striking differences in the observed morphological anisotropy provides an initial indication that dynamic scaling parameters are not identical between the two thickness series.

V. SCALING AND ROUGHNESS ASSESSMENT

What follows is a summary of the results of the scaling analysis applied to Series 1 and Series 2 films [20]. The global roughness scaling parameters were extracted from the AFM scans from each thickness series. A 2D autocorrelation function was applied to the AFM images and provided a means for identifying the anisotropic average island size by fitting the average features to Gaussians and calculating their FWHM value [21]. The results for each film series are reported in Table I.

For film Series 1, the nature of the observed anisotropy is biaxial; hence, the autocorrelation function, which was taken along the fast scan direction, is a convolution of the average island size along the major and minor anisotropy axes. As such, it is necessary in this case to define two separate dynamic scaling parameters. Fitting a convolution of Gaussians allows for the determination of global, anisotropic values for β/α. Hence, the values $(\beta/\alpha)_{\text{width}} = 0.40$ and $(\beta/\alpha)_{\text{length}} = 0.55$ ("width" corresponding to the minor island morphological axis and "length" corresponding to the major island morphological axis) as well as $\beta = 0.60$ were found while anisotropic values for global α were calculated to be $\alpha_{\text{length}} = 1.1$ and $\alpha_{\text{width}} = 1.5$ with an average $\alpha_{\text{avg}} = 1.3$, which was derived from a radial average of the autocorrelation function. Local scaling parameters were obtained via real space methods by analyzing short line scans constrained along the tops of the morphological islands. The local values $\alpha_{\text{loc}} = 0.56$ and $\beta_{\text{loc}} = 0.34$ were obtained. Here we see clear deviation between the local and calculated global scaling parameters indicating *anomalous scaling*.

TABLE I. Overview of scaling results for each thin film thickness series.

	Series 1 (bicrystal)	Series 2 (single crystal)
β/α	0.40–0.55	0.31
β	0.60	1.3
α	1.1–1.5	4.3
α_s	1.4	1.2
α_{loc}	0.56	···
β_{loc}	0.34	···
Universality class	Super-rough	New-class

The spectral exponent, extracted from a linear fit in the regime of large k from the PSD log-log plot (Fig. 7), was determined from the thickest film, $\alpha_s = 1.4$, and is near the average value for the global static coarsening exponent. In the context of general dynamic scaling, for this particular set of deposition parameters, the surface of Nb(110)/MgO(001) scales as the *super-rough scaling*

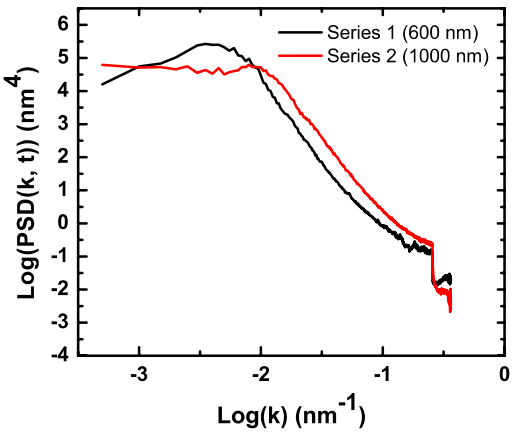

FIG. 7. PSD curves for the thickest Nb samples from each series.

universality class, which is characterized by a surface which tends to dramatically coarsen even at large film thicknesses where a saturation of roughness could ordinarily be expected (as is the case with Family-Vicsek scaling). Evidently, this suggests an undesirable growth mode for the application of these thin films for multilayer SIS structures.

Scaling parameters for Series 2 films were similarly extracted from the corresponding AFM images. Because of the isotropic nature of the surface features, only average features were considered for the determination of scaling parameters. Furthermore, because of the relatively fine surface features, the real space methods used to collect local scaling features previously used in Series 1 films were not applicable. Hence, here we report only global scaling information for Series 2 films. A global coarsening parameter $\alpha = 4.3$ was calculated from the measured scaling parameters of $\beta/\alpha = 0.31$ and $\beta = 1.3$. This rather large value for α deviates significantly with the $\alpha_s = 1.26$, extracted from the PSD from the best fit slope along the linear region of the thickest film, and suggests that the dynamical evolution of the Nb(100)/MgO(001) under these growth condition follows the *new-class* universality class that indicates a set of deposition conditions leading to a comparatively more desirable surface for the proposed application.

VI. CORRELATION BETWEEN SURFACE, MICROSTRUCTURE, AND SUPERCONDUCTING PROPERTIES

To correlate our assessment based on surface roughness analysis with physical properties relevant to the proposed application in SRF cavities, we have also measured relevant superconducting properties. Thus, we have determined the residual resistance ratio (RRR), which is the ratio of resistance at 300 K (room temperature) to the resistance at 10 K (slightly above T_C). In fact, the value of RRR is an indication of the purity and the low-temperature thermal conductivity of the niobium, and is often used as a material specification for SRF applications. Lower values of RRR indicate a greater concentration of imperfections. Here, resistance measurements were carried out using a four-point probe setup in the 6–300 K temperature range for representative films with similar thickness ($\sim$ 600 nm) grown with the characteristic morphological and structural characteristics from each series. Figure 8 shows the results for one such typical measurement for a 600 nm film from Series 2. The T_C for the niobium films was found to be $\sim$9.2 K. We found that resistivity data are consistent with our surface assessment, since lower RRR values were obtained for rougher films; thus, the RRR values were 46.5 for the Series 1 film and 165.5 for Series 2 film. Epitaxial films from Series 2 tend towards smoother surfaces and higher RRR as compared to the epitaxial thin film Series 1 counterparts. We note that the RRR value of the thickest film in Series 2 compares very favorably with the values found for films of similar thickness grown with higher energetic beams [3].

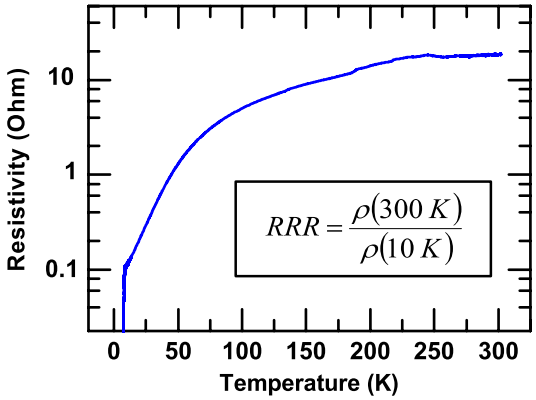

FIG. 8. Resistivity as a function of temperature in a 600 nm, single crystal Nb(001)/MgO(001) film.

VII. CONCLUSIONS

We have shown that the epitaxial growth of Nb films onto MgO(001) substrates can exhibit one of two distinct crystallographic registries depending on the nucleation conditions and that morphology anisotropies and dynamical evolution of the surfaces, within the context of general dynamical scaling, are correlated with the observed crystallographic anisotropies. For our set of growth parameters, the Nb(100)/MgO(001) surface scales as a super-rough universality class and the Nb(110)/MgO(001) surface scales as a "new-class" universality class. Pursuant to practical considerations for the development of Nb/MgO/Nb SIS multilayers, the relatively low rms roughness of the Nb surface for thick films of Nb(001)/MgO(001), as compared with the thick films of Nb(110)/MgO(001), makes it a more desirable candidate in terms of minimizing surface roughness under these growth conditions, potentially leading to suitable templates for multilayers geared toward improved SRF multilayer surfaces and performance. Thus, our studies provide a suitable framework to characterize the surface morphology and its correlation with transport properties for films grown with different techniques aiming at improved SRF applications.

ACKNOWLEDGMENTS

This work was funded by the Defense Threat Reduction Agency (HDTRA1-10-1-0072) and the U. S. Department of Energy (DE-AC05-06OR23177).

[1] C. Benvenuti, N. Circelli, and M. Hauer, Appl. Phys. Lett. **45**, 583 (1984).
[2] S. Calatroni, Physica (Amsterdam) **441C**, 95 (2006).
[3] M. Krishnan, E. Valderrama, C. James, X. Zhao, J. Spradlin, A.-M. Feliciano, L. Phillips, C. Reece, K. Seo,

and Z. Sung, Phys. Rev. ST Accel. Beams **15**, 032001 (2012).
[4] V. G. Kogan and N. Nakagawa, Phys. Rev. B **35**, 1700 (1987).
[5] A. Gurevich, Appl. Phys. Lett. **88**, 012511 (2006).
[6] Chen Xu, Hui Tian, Charles E. Reece, and Michael J. Kelley, Phys. Rev. ST Accel. Beams **14**, 123501 (2011).
[7] A. P. Ehiasarian, R. New, W.-D. Münz, L. Hultman, U. Helmersson, and V. Kouznetsov, Vacuum **65**, 147 (2002).
[8] J. A. Thornton, J. Vac. Sci. Technol. **11**, 666 (1974).
[9] A. Anders, Thin Solid Films **518**, 4087 (2010).
[10] N. Martin and C. Rousselot, J. Appl. Phys. **87**, 8747 (2000).
[11] Xin Ge and Karina Morgenstern, Phys. Rev. B **85**, 045417 (2012).
[12] B. Wiedenhorst, C. Hofener, Y. Lu, J. Klein, L. Alff, R. Gross, B. H. Freitag, and W. Mader, Appl. Phys. Lett. **74**, 3636 (1999).
[13] John E. Mahan, Kent M. Geib, G. Y. Robinson, and Robert G. Long, J. Vac. Sci. Technol. A **8**, 3692 (1990).
[14] R. Droopad, R. L. Williams, and S. D. Parker, Semicond. Sci. Technol. **4**, 111 (1989).
[15] C. Clavero, D. B. Beringer, W. M. Roach, J. R. Skuza, K. C. Wong, A. D. Batchelor, and R. A. Lukaszew, Cryst. Growth Des. **12**, 2588 (2012).
[16] I. Horcas, R. Fernandez, J. M. Gomez-Rodriguez, J. Colchero, J. Gomez-Herrero, and A. M. Baro, Rev. Sci. Instrum. **78**, 013705 (2007).
[17] F. Family and T. Vicsek, J. Phys. A **18**, L75 (1985).
[18] J. J. Ramasco, J. M. Lopez, and M. A. Rodriquez, Phys. Rev. Lett. **84**, 2199 (2000).
[19] T. E. Hutchinson, J. Appl. Phys. **36**, 270 (1965).
[20] D. B. Beringer, W. M. Roach, C. Clavero, C. E. Reece, and R. A. Lukaszew, "Surface roughness scaling analysis applied to thin films for SRF applications," Phys. Rev. B (to be published).
[21] M. A. Auger, L. Vazquez, R. Cuerno, M. Castro, M. Jergel, and O. Sanchez, Phys. Rev. B **73**, 045436 (2006).